Monthly Notices
of the
ROYAL ASTRONOMICAL SOCIETY
MNRAS **457,** 2988–2998 (2016) doi:10.1093/mnras/stw176

Broad-band spectral analysis of the accreting millisecond X-ray pulsar SAX J1748.9−2021

F. Pintore,[1,2]★ A. Sanna,[1] T. Di Salvo,[3] M. Del Santo,[4] A. Riggio,[1] A. D'Aì,[4] L. Burderi,[1] F. Scarano[1] and R. Iaria[3]

[1]*Università degli Studi di Cagliari, Dipartimento di Fisica, SP Monserrato-Sestu, KM 0.7, I-09042 Monserrato, Italy*
[2]*INAF – Istituto di Astrofisica Spaziale e Fisica Cosmica – Milano, via E. Bassini 15, I-20133 Milano, Italy*
[3]*Dipartimento di Fisica e Chimica, Università di Palermo, via Archirafi 36, I-90123 Palermo, Italy*
[4]*INAF – Istituto di Astrofisica Spaziale e Fisica Cosmica – Palermo, via U. La Malfa 153, I-90146 Palermo, Italy*

Accepted 2016 January 19. Received 2016 January 15; in original form 2015 September 10

ABSTRACT

We analysed a 115-ks *XMM–Newton* observation and the stacking of 8 d of *INTEGRAL* observations, taken during the raise of the 2015 outburst of the accreting millisecond X-ray pulsar SAX J1748.9−2021. The source showed numerous type-I burst episodes during the *XMM–Newton* observation, and for this reason we studied separately the persistent and burst epochs. We described the persistent emission with a combination of two soft thermal components, a cold thermal Comptonization component (∼2 keV) and an additional hard X-ray emission described by a power law ($\Gamma \sim 2.3$). The continuum components can be associated with an accretion disc, the neutron star (NS) surface and a thermal Comptonization emission coming out of an optically thick plasma region, while the origin of the high-energy tail is still under debate. In addition, a number of broad ($\sigma = 0.1$–0.4 keV) emission features likely associated with reflection processes have been observed in the *XMM–Newton* data. The estimated 1.0–50 keV unabsorbed luminosity of the source is $\sim 5 \times 10^{37}$ erg s^{-1}, about 25 per cent of the Eddington limit assuming a 1.4 M$_\odot$ NS. We suggest that the spectral properties of SAX J1748.9−2021 are consistent with a soft state, differently from many other accreting X-ray millisecond pulsars which are usually found in the hard state. Moreover, none of the observed type-I burst reached the Eddington luminosity. Assuming that the burst ignition and emission are produced above the whole NS surface, we estimate an NS radius of ∼7–8 km, consistent with previous results.

Key words: accretion, accretion discs – X-rays: binaries – X-rays: galaxies – X-rays: individual: SAX J1748.9−2021.

1 INTRODUCTION

After the discovery, in 1998, of SAX J1808.4−3658 (Wijnands & van der Klis 1998), the first accreting neutron stars (NS) hosted in a low-mass X-ray binary (LMXB) system and showing a spin pulsation of the order of the millisecond, the class of the accreting X-ray millisecond pulsars (AMXPs) increased nowadays up to 17 sources, including the transitional millisecond pulsars PSR J1023+0038 (Archibald et al. 2015) and XSS J12270 (Papitto et al. 2013b). Their spectral and temporal properties have been widely investigated (see Patruno & Watts 2012; Burderi & Di Salvo 2013, and reference therein, for recent reviews), proving that the matter in the accretion disc around the NS can exert a torque able to accelerate the NS spin period down to a few milliseconds (1.6–5.5 ms the pulsation range of those currently detected). When the magnetic field of the NS is strong enough (estimated values are between 10^8 and 10^9 G), it is able to force at least part of the accreting matter towards the magnetic NS polar caps. The X-ray photons created by the release of energy above the NS surface are then observed in terms of pulsation. The millisecond pulsation frequency, reached by the transfer of angular momentum provided by the accreting matter on to the NS (see e.g. Bhattacharya & van den Heuvel 1991 for a review), can be then seen thanks to the offset angle between the rotation axis and the magnetic axis. Because of the magnetic field, the accretion disc can be truncated at the so-called magnetospheric radius, usually expressed in terms of a fraction of the Alfvén radius (Ghosh & Becker 2008). Investigations on the values assumed by the truncation radius were carried out by studies of both timing and spectral properties (e.g. Burderi & King 1998; Papitto et al. 2009; Patruno et al. 2009b; Cackett et al. 2010; Wilkinson et al. 2011). In particular, from a spectral point of view, an estimate on the inner

★ E-mail: pintore@iasf-milano.inaf.it

© 2016 The Authors
Published by Oxford University Press on behalf of the Royal Astronomical Society

Downloaded from https://academic.oup.com/mnras/article-abstract/457/3/2988/2588964 by Fabio Pintore on 09 May 2020

disc radius can be provided by the analysis of broad emission lines often seen in the spectra of AMXPs. These are usually observed at the energies of the K-shell iron transitions (6.4–7.0 keV) and likely produced by reflection off of hard photons from the surface of the accretion disc. In particular, the broadening of these lines is commonly explained with relativistic effects associated with the fast rotation of the accretion disc in the proximity of the strong gravitational field of the compact object (e.g. Papitto et al. 2009; Cackett et al. 2010). Therefore, from the shape of the emission feature, it is possible to trace the location of the radius of the accretion disc where the line is formed. In addition to these features, AMXP spectra are often characterized by a multicolour blackbody emitted from the accretion disc and a Comptonized emission probably produced in the regions closer to the NS, as the boundary layer (e.g. Papitto et al. 2009). In some cases, an additional soft blackbody component is detected and likely associated with the NS surface emission (e.g. Poutanen 2006).

For this subclass of X-ray systems, generally the coherent NS pulsation is persistent during the source outbursts, with the exception of three AMXPs (Aql X-1, HETE 1900.1−2455 and SAX J1748.9−2021) that showed intermittent pulsations whose origin is still uncertain (Kaaret et al. 2006; Galloway et al. 2007; Gavriil et al. 2007; Altamirano et al. 2008; Casella et al. 2008; Papitto et al. 2013a; Messenger & Patruno 2015). In this work, we focus on the AMXP SAX J1748.9−2021, discovered by *BeppoSAX* during the 1998 outburst, located in the globular cluster NGC 6440 (in't Zand et al. 1999) at a distance of ∼8.5 and 0.6 kpc above the Galactic plane (Martins, Harvel & Miller 1980; Ortolani, Barbuy & Bica 1994; Kuulkers et al. 2003; Valenti, Ferraro & Origlia 2007). Several outbursts were observed in 1998, 2001, 2005 and 2010 (in't Zand et al. 1999, 2001; Verbunt et al. 2000; Markwardt & Swank 2005; Patruno et al. 2009a) and a probable outburst in 1971 (Markert et al. 1975) was a posteriori associated with the source. During the quiescence of the source, in't Zand et al. (2001) were also able to univocally detect the companion star and Altamirano et al. (2008) estimated its mass range (0.1–1 $M_{\odot}$). SAX J1748.9−2021 showed an intermittent pulsation at 442.361 Hz from which it was possible to infer an orbital period of ∼8.76 h and a projected semimajor axis of ∼0.4 light-seconds (Altamirano et al. 2008; Patruno et al. 2009a). Finally, a number of type-I X-ray bursts were found with the *Rossi X-ray Timing Explorer* (*RXTE*), which presented a blackbody emission of a few keV temperatures evolving during the thermonuclear flashes produced on the NS surface (Galloway et al. 2008).

In this work, we investigate the broad-band spectral properties of the source SAX J1748.9−2021 making use of a very high quality *XMM–Newton* observation and the stacking of *INTEGRAL* observations during the 2015 outburst. The source went in outburst on February 17th and first detected by *INTEGRAL* (Bozzo, Kuulkers & Ferrigno 2015a; Kuulkers et al. 2015). Type-I X-ray bursts were also observed during later *INTEGRAL* observations (Bozzo, Falanga & Ferrigno 2015b). The whole outburst lasted for about 60 d, and it was largely monitored by *Swift*/X-Ray Telescope (XRT). The spectral capabilities of *XMM–Newton* provide a powerful insight for the investigation of the X-ray emission of this object, and also allow refined studies of the iron emission line and other discrete features in this source.

2 DATA REDUCTION

We analysed an *XMM–Newton* observation taken on 2015 March 4 (Obs.ID. 0748391301) obtained with a Target of Opportunity (ToO) at the beginning of the 2015 outburst, and the whole available 2015 *INTEGRAL* data set between March 5 and 13.

The *XMM–Newton* observation was made in both TIMING (∼100 ks) and BURST (∼10 ks) mode for the European Photon Imaging Camera (EPIC)-pn. The reading times of the two modes are 30 and 7 μs, respectively, although for the BURST mode only the 3 per cent of the incident photons are collected. EPIC-MOS1 and EPIC-MOS2 were instead operating in TIMING and IMAGING mode, respectively. Data from all *XMM–Newton* instruments were reduced using the up-to-date calibration files and the Science Analysis Software (SAS) v. 14.0.0 and adopting the standard reduction pipeline RDPHA (XMM-CAL-SRN-0312;[1] see also Pintore et al. 2014). Because of severe pile-up in the EPIC-MOS data, which cannot be corrected by adopting the standard procedure of removing central columns (or pixels) of the CCD, we do not consider them in our analysis. The last 5 ks of the TIMING mode EPIC-pn observation were affected by high solar background, hence we removed them from the analysis. EPIC-pn spectra were extracted selecting events with PATTERN ≤4, which allows for single and double pixel events, and 'FLAG=0', which retains events optimally calibrated for spectral analysis. We remark that the EPIC-pn count rate observed during the TIMING mode is, on average, higher than 700 counts s^{-1}, and hence the *counting mode* was often triggered especially during the type-I bursts, limiting our studies on them. Because of the high count rate of the source, pile-up effects are not negligible. In order to investigate pile-up effects in the data, we compared the spectrum extracted taking into account all the columns of the CCD in the range RAWX = [31:43] with spectra obtained excising one, three and five central brightest columns of the aforementioned RAWX range. We found that pile-up effects can be strongly limited by excising only the central column RAWX = 37, therefore, hereafter we will refer to the spectrum extracted in the range RAWX = [31:43] without the central column. The background spectrum was instead extracted in the RAWX range [3:5]. We checked that the background extracted in this region was not heavily contaminated by the source, comparing it with the local background estimated during an *XMM–Newton* observation when the source was in quiescence. The response matrix and the ancillary file were created following the standard procedure for the pile-up correction. The EPIC-pn spectrum was finally rebinned with an oversample of three channels per energy resolution element using the SPECGROUP task.

The reduction of Reflection Grating Spectrograph (RGS) spectra, first and second order, was carried out adopting the standard RGSPROC task, filtering for high background intervals. Pile-up effects are not negligible because the RGS1 and RGS2 fluxes indicate that the nominal pile-up threshold is overcame. In more detail, the inferred flux in the 0.3–2.0 keV (see Section 6) for both instruments is ∼5.2 × 10^{-10} and ∼4.9 × 10^{-10} erg cm^{-2} s^{-1} (adopting a simple power-law model) which is well above the pile-up threshold of RGS1 and RGS2 reported by the *XMM–Newton* user manual (∼3 × 10^{-10} and ∼1.5 × 10^{-10} erg cm^{-2} s^{-1}, respectively). Because pile-up in RGS cannot be easily solved, we will analyse RGS data separately from the EPIC-pn and *INTEGRAL* spectra. We create an average spectrum stacking together the RGS1 and RGS2 data and, adopting the tool RGSCOMBINE which combines, separately, first- and second-order spectra, we rebin the data with at least 1000 counts bin^{-1}. Because the background is dominant below 0.75 keV, we analyse the energy range 0.75–2.0 keV.

[1] http://xmm2.esac.esa.int/docs/documents/CAL-SRN-0312-1-4.pdf

Downloaded from https://academic.oup.com/mnras/article-abstract/457/3/2988/2588964 by Fabio Pintore on 09 May 2020

We searched for all the available *INTEGRAL* observations performed in 2015 between March 5 and 13. In order to maximize the Imager on Board the *INTEGRAL* Satellite (IBIS)/*INTEGRAL* Soft Gamma-Ray Imager (ISGRI; Lebrun et al. 2003) and Joint European X-Ray Monitor (JEM-X; Lund et al. 2003) spectral responses, we selected only pointings (i.e. science windows, SCW, with typical duration of 2 ks) with the source located within 7°.5 and 3°.5 from the centre of the IBIS and JEM-X field of views (FOV), respectively. Since the single observations do not show significant spectral variability amongst them (apart for flux changes), we stacked 16 SCWs for IBIS/ISGRI and three for JEMX-1 and JEMX-2 which have been analysed by using version 10.1 of the OSA software distributed by the *INTEGRAL* Science Data Centre (ISDC; Courvoisier et al. 2003). Because of the faintness of the source in hard X-rays (about 10 mCrab, or $\sim 8 \times 10^{-11}$ erg cm^{-2} s^{-1}, in 20–40 keV), the ISGRI spectrum has been extracted by the total mosaic image with the MOSAIC_SPEC tool in three energy bins spanning from 20 up to 60 keV. However, the source is very bright (about 100 mCrab) in the soft X-rays. The source spectrum could be extracted from mosaic images of the two cameras of the JEM-X telescope, i.e. JEMX-1 and JEMX-2. First we produced images for each SCW in 16 narrow energy bands (from 3 to 35 keV) and then we extracted the spectrum by the total image with the MOSAIC_SPEC TOOL. However, according to the *INTEGRAL* calibration team, spectra are actually well calibrated in the range 7–25 keV, thus the final JEM-X spectra have only seven bins. The total good time intervals of the IBIS/ISGRI and JEM-X spectra are 30.5 and 5.1 ks, respectively.

We fit simultaneously the *XMM–Newton* (EPIC-pn) and *INTEGRAL* (JEMX-1, JEMX-2 and ISGRI) spectra, using XSPEC v. 12.8.2 (Arnaud 1996). We select the energy ranges 1.0–10.0, 7.0–25.0 and 20.0–50.0 keV, for EPIC-pn, JEMX-1/X2 and ISGRI spectra, respectively. We ignore the EPIC-pn channels at energies lower than 1.0 keV as calibrations in TIMING mode are still uncertain below this energy (internal *XMM–Newton* report CAL-TN-0083).[2] We also consider a systematic error of 0.15 and 2 per cent for the EPIC-pn and *INTEGRAL* spectra, respectively.

3 SPECTRAL ANALYSIS

The *XMM–Newton* observation caught SAX J1748.9−2021 during the initial phases of the outburst, approximately at half of the peak luminosity. The peak was instead caught by the *INTEGRAL*-ISGRI and *INTEGRAL*-JEMX observations (see Fig. 1). In the *XMM–Newton* observation, SAX J1748.9−2021 showed 25 type-I bursts during the EPIC-pn TIMING mode (see Fig. 2) and two during the EPIC-pn BURST mode. Since X-ray bursts affect the spectral properties of the persistent emission of the source (see the hardness ratios variability showed in Fig. 3), we first focus our spectral analysis on the persistent emission (i.e. without bursts), in Section 3.1, and subsequently we investigate the properties of the type-I bursts in Section 3.3. We note that the persistent emission does not show short-term spectral variability during the observation, hence, hereafter we will refer only to the average persistent spectrum. In addition, because of the very poor counting statistics of the EPIC-pn BURST mode, we limit our analysis of the persistent epochs to the EPIC-pn TIMING mode only and we use both modes for the type-I burst analysis. We finally note that no bursts are found during the *INTEGRAL*/JEM-X considered SCWs and that no spectral variability was found between EPIC-pn and *INTEGRAL* spectra, as the best-fitting spectral model for the broad-band spectra (see Section 3.1) can also well fit the EPIC-pn spectrum alone.

[2] http://xmm2.esac.esa.int/docs/documents/CAL-TN-0083.pdf

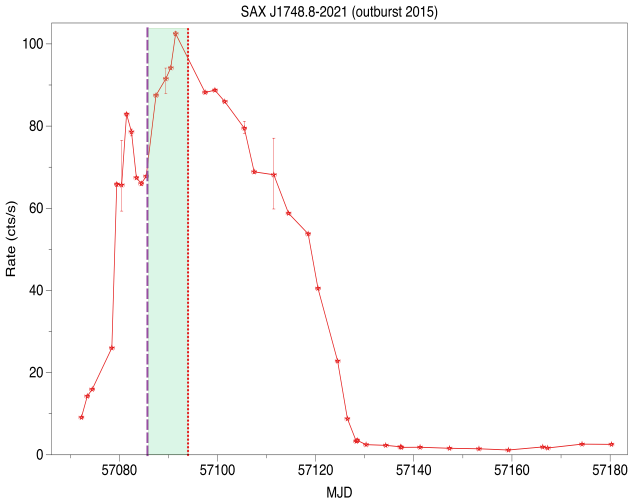

Figure 1. *Swift*-XRT light curve of the 2015 outburst of SAX J1748.9−2021. The violet dashed line indicates the epoch of the *XMM–Newton* observation, the red dotted line is the epoch of the *INTEGRAL*/JEM-X observation, while the green area represents the observation epochs of *INTEGRAL*/ISGRI.

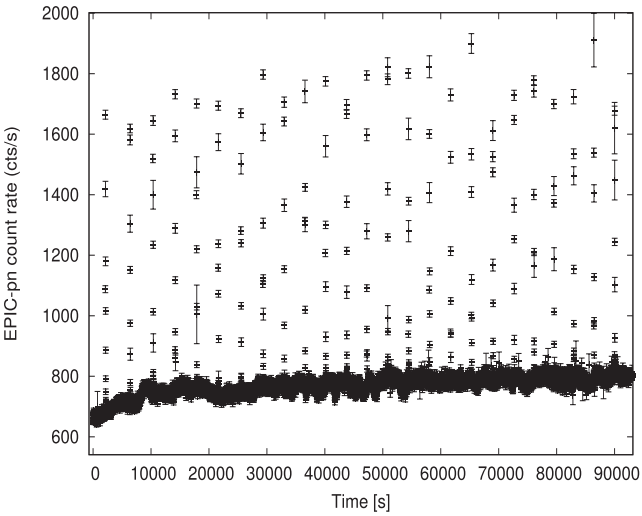

Figure 2. *XMM–Newton* EPIC-pn 0.3–10 keV light curve of SAX J1748.9−2021 after the removal of the latest 10 ks of data affected by high solar background. 25 type-I X-ray bursts were detected during the observation.

3.1 Persistent emission

We initially fit EPIC-pn and *INTEGRAL* data together with a simple absorbed (TBABS in XSPEC) multicolour blackbody disc (DISKBB; Mitsuda et al. 1984) plus a thermal Comptonization model (NTHCOMP; Zdziarski, Johnson & Magdziarz 1996; Życki, Done & Smith 1999). We adopt the abundances of Anders & Grevesse (1989) and the cross-sections of Balucinska-Church & McCammon (1992). For each spectrum, we add a multiplicative constant which takes into account the different cross calibrations of the instruments. In addition, we note that the disc temperature and the seed photons temperature for Comptonization are very similar, hence we keep them tied (i.e. assuming that the soft component is the source of

Downloaded from https://academic.oup.com/mnras/article-abstract/457/3/2988/2588964 by Fabio Pintore on 09 May 2020

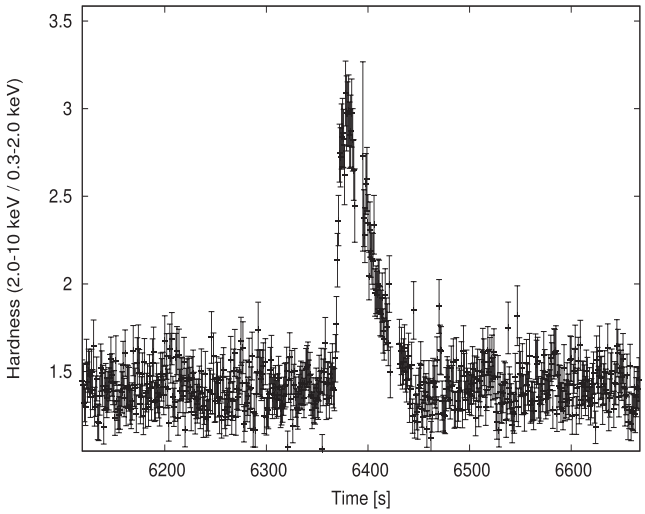

Figure 3. Hardness ratio of the 2.0–10.0 and 0.3–2.0 keV *XMM–Newton* EPIC-pn light curves of SAX J1748.9−2021, around a type-I burst. Time is calculated from the beginning of the *XMM–Newton* observation. The hardness ratio is quite constant during the persistent emission, but clear variability is introduced during the burst episode.

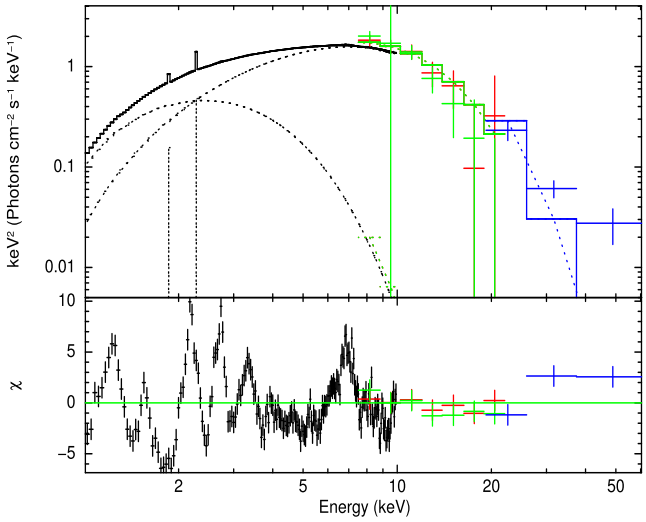

Figure 4. Unfolded $E^2f(E)$ *XMM–Newton*/EPIC-pn (black), *INTEGRAL*/JEMX-1 (red) and JEMX-2 (green), and *INTEGRAL*/ISGRI (blue) fitted with absorbed DISKBB and NTHCOMP components. Several features in the EPIC-pn spectrum are observed across the 0.3–10 keV; an excess is also found above 20 keV in the ISGRI spectrum (see text).

seed photons). We clearly identify structures in the EPIC-pn residuals, likely associated with emission features. Because the EPIC-pn spectra taken in TIMING mode are affected by systematic emission features at 1.8–1.9 and 2.2–2.3 keV produced by instrumental Si and Au edges, hereafter we will include two narrow Gaussian emission lines in the model. We find that the fit with this model is statistically poor and leaves several residuals (Fig. 4) associated with broad emission features and with an excess in the ISGRI data, meaning that at least an additional component is requested for the continuum.

We initially model the broad iron emission feature, found at ∼6.75 keV. Because of its broadness ($\sigma \sim 0.4$ keV), we fit it alternatively with a GAUSSIAN model or with a relativistically smeared reflection profile (DISKLINE; Fabian et al. 1989), the latter in order to take into account probable effects due the fast rotation of the matter in the disc if the line was produced by reflection off of hard photons from the surface of the inner disc. We find that, although the introduction of a GAUSSIAN model is statistically significant, the DISKLINE provides a marginally better fit to the data ($\Delta\chi^2 = 220.89$ for three additional dof versus $\Delta\chi^2 = 242.44$ for five additional dof, respectively). Moreover, the DISKLINE model allows us to find a coherent picture with the disc model (see below). For this reason, in the following, we adopt the DISKLINE model for the iron line. Because the fit is insensitive to the parameter, we fix the outer disc radius to 10^5 gravitational radii ($R_g = GM/c^2$ where G is the gravitational constant, M is the NS mass and c is the speed of light). The energy of the iron emission feature (∼6.7/6.8 keV) is consistent with a Fe XXV Kα line (equivalent width, EW, of ∼30 eV), produced in the disc at a distance of ∼20–43R_g. In addition, from the line, we can also constrain the inclination angle of the system being in the range 38°–45°. On the other hand, we note that the gravitational radius at which the reflection line should have been produced (20–43R_g) is not consistent with the inner disc temperature (∼1.2 ± 0.1 keV), which instead suggests an inner disc radius of (6–8)/cos(θ) km (where θ is the inclination angle, and it cannot be likely higher than 70°–75° as no eclipses are seen for this source), thus apparently below the latest stable orbit and physically not realistic.

The combination of a small inner disc radius, a high temperature and the discrepancy with the DISKLINE inner radius makes the fit with a single soft component unlike. A more physical spectral description suggests instead that the soft component may be split in two components, a multicolour blackbody (DISKBB) to model the emission from the accretion disc, and a blackbody to model the emission from the NS surface. For this model, we keep linked the blackbody temperature and the seed photons temperature of the NTHCOMP. We find an absorption neutral column density of $nH \sim 5.8 \times 10^{21}$ cm^{-2} (about a factor of 2 higher than the average Galactic extinction in the direction of the source, 3.29×10^{21} cm^{-2}; Dickey & Lockman 1990), an inner disc temperature of $kT_{\rm disc} \sim 0.95$ keV, a NS surface temperature of $kT_{\rm disc} \sim 1.1$ keV and an electron temperature of the Comptonizing plasma of $kT_{\rm e} \sim 2.1$ keV with an asymptotic power-law photon index <1.1. These spectral parameters suggest that the source was observed during a soft state. The radius related to the emission of the BBODY component is consistent with either the NS surface or a region very close to the NS ($R = 7 \pm 3$ km). From the DISKBB temperature (which, taking into account the uncertainties, can be as low as 0.6 keV) normalization is possible to determine an upper value to the inner disc radius of $R_{\rm in} \sim 15$ km (for an inclination of 37°–56°, 90 per cent error, and not corrected for any colour temperature factor) which could be compared to the lower limit of the inner disc radius inferred by the DISKLINE model (∼38 km).

However, residuals are still observed at very high energy in the ISGRI spectrum. Since hard power-law tails are often found in the spectra of Galactic black hole (e.g. McClintock & Remillard 2006; Del Santo et al. 2015) and NS X-ray binary systems (e.g. Di Salvo et al. 2000, 2001, 2006; Iaria et al. 2004; Paizis et al. 2006; D'Aí et al. 2007; Piraino et al. 2007; Tarana et al. 2007; Del Santo et al. 2008; Bouchet et al. 2009; Del Santo 2012), we add a POWER-LAW (in XSPEC) component to the total model. This component is able to flatten the higher energy residuals and it is statistically significant ($\Delta\chi^2 = 17$ for 2 additional dof). This finding indicates that the thermal Comptonization component alone is not able to describe the hard X-rays emission while a further non-thermal component is necessary. The physical meaning of additional hard X-ray power laws in spectra of XRBs is still matter of debate. They have been associated with either emission of Comptonization by a non-thermal

Downloaded from https://academic.oup.com/mnras/article-abstract/457/3/2988/2588964 by Fabio Pintore on 09 May 2020

medium (Poutanen & Coppi 1998) or bulk motion of accreting material close to the NS (e.g. Titarchuk & Zannias 1998, but see also Di Salvo et al. 2000). We verified that such a feature is not due to the predominance of the EPIC-pn spectrum guiding the fit: by excluding the EPIC-pn spectrum and fitting simultaneously only the ISGRI, JEMX-1 and JEMX-2 data, we can still find evidence of this hard tail. Moreover, we tried with a COMPPS model (Poutanen & Svensson 1996) fitting the *INTEGRAL* data assuming both the Maxwellian electron distribution and the hybrid (thermal/non-thermal) distribution. We found that the fit is statistically acceptable only when using the hybrid model. However, because of the low statistics at high energy, we did not manage to constrain the electron power-law index.

The interpretation of the continuum provides a coherent picture of the accretion mechanisms of the source. In fact, millisecond coherent pulsations at ∼442 Hz have been found in the *XMM–Newton* observation (Sanna et al., submitted), pointing towards a magnetically driven accretion column on to the NS polar caps, which produces most of the blackbody emission. In addition, this scenario rules out the possibility that the disc reached the last stable orbit, where the magnetic lines cannot channel the matter anymore towards the polar caps, but instead supports a truncated accretion disc, as that inferred in the best-fitting continuum model.

In addition to the continuum, we also mention that emission features with centroid energy of 1.23, 1.56, 2.18, 2.7, 3.29 and 3.98 keV are found; however, the lines at 1.56 and 2.18 keV are likely dubbed instrumental as the former (probably Al) has a broadening consistent with 0, while the latter is not easily associated with any of the known X-ray transitions of the most abundant elements. In particular, the 2.18 keV line is close to the Au instrumental edge of the EPIC-pn, and therefore it may be due to a miscalibration of the response matrix in the 2.2–2.3 keV energy range. The other lines may be instead associated with K-shell emission lines of Na IX (1.237 keV), S XVI (2.62 keV), Ar XVIII (3.32 keV) and Ca XX or Ca xix (4.11 or 3.90 keV). However, we are suspicious about the Na IX line as the chemical abundance of this element is low if compared to the ionized transitions of other more abundant elements which can show emission line at energies <2 keV (e.g. Mg XI, H- and He-like lines at ∼1.47 and ∼1.35 keV, respectively). On the other hand, we note that the neutral Mg has a Kα transition at 1.25 keV: if the observed line is associated with neutral Mg, we suggest that such a line is produced in a different region than the other emission features. Hereafter we limit our discussion to the lines of S, Ar and Ca: their broadening is usually lower than 0.2 keV (see Table 1) and their EW is consistent with ∼10, ∼10 and ∼2 eV, respectively. Because the broadening of the Fe, Ar, Ca and S lines is similar to that of the iron line, we tentatively describe also the low-energy lines with DISKLINE models, linking all the relativistic parameters to those of the iron DISKLINE component (as in di Salvo et al. 2009). However, this approach provides a poorer fit with respect to GAUSSIAN models applied to the low-energy lines, $\chi^2_\nu = 1.22$ versus $\chi^2_\nu = 1.1$; in particular, with respect to the continuum model without the low-energy emission lines, the *F*-test probability of chance improvement is $<3 \times 10^{-37}$ and $<4.9 \times 10^{-40}$ when adopting DISKLINE and GAUSSIAN models, respectively. Furthermore, we note that, directly comparing the GAUSSIAN and DISKLINE models, the former is statistically better with an *F*-test probability of chance improvement $<2 \times 10^{-5}$. Hence, hereafter, we will only discuss the fit with the low-energy lines fitted with GAUSSIAN models. The final fit is clearly robust and well describes the broadband spectrum (χ^2/dof = 199.53/183). We report the best-fitting

Table 1. Best-fitting spectral parameters obtained with the absorbed continuum BBODY+DISKBB+NTHCOMP+POWER-LAW model, plus an absorption edge and six emission lines. Errors are at 90 per cent for each parameter.

Model	Component	
TBABS	nH (10^{22} cm^{-2})[a]	$0.56^{+0.05}_{-0.03}$
DISKBB	$kT_{\rm disc}$ (keV)[b]	$0.95^{+0.5}_{-0.4}$
	Norm[c]	108^{+54}_{-15}
BBODY	$kT_{\rm bb}$ (keV)[d]	$1.08^{+0.2}_{-0.06}$
	Radius (km)[e]	7 ± 3
NTHCOMP	$\Gamma_{\rm compt}$[f]	<1.07
	$kT_{\rm e}$ (keV)[g]	$2.10^{+0.1}_{-0.08}$
	Norm(10^{-3})[h]	9^{+40}_{-2}
POWER-LAW	Γ[i]	2.3 ± 0.2
	Norm[j]	$0.066^{+0.068}_{-0.065}$
EDGE	Energy (keV)[k]	8.7 ± 0.1
	τ[l]	0.022 ± 0.006
DISKLINE	Energy (keV)[m]	$6.79^{+0.05}_{-0.06}$
	β[n]	$-2.7^{+0.1}_{-0.2}$
	$R_{\rm in}$ ($R_{\rm g}$)[o]	29^{+12}_{-9}
	$R_{\rm out}$ ($R_{\rm g}$)[p]	10^5 (frozen)
	Inclination (°)[q]	44^{+10}_{-6}
	Norm (10^{-4})[r]	$9.9^{+1.6}_{-1.3}$
GAUSSIAN	Energy (keV)[s]	1.23 ± 0.02
	σ (keV)[t]	$0.06^{+0.03}_{-0.3}$
	Norm (10^{-3})[u]	$1.5^{+0.8}_{-0.5}$
GAUSSIAN	Energy (keV)[s]	1.56 ± 0.01
	Norm (10^{-4})[u]	$5.9^{+1.4}_{-1.3}$
GAUSSIAN	Energy (keV)[s]	$2.187^{+0.008}_{-0.009}$
	σ (keV)[t]	0.11 ± 0.01
	Norm(10^{-3})[u]	2.4 ± 0.3
GAUSSIAN	Energy (keV)[s]	2.698 ± 0.009
	σ (keV)[t]	$0.096^{+0.013}_{-0.006}$
	Norm (10^{-3})[u]	$1.7^{+0.2}_{-0.1}$
GAUSSIAN	Energy (keV)[s]	3.29 ± 0.02
	σ (keV)[t]	$0.17^{+0.03}_{-0.02}$
	Norm (10^{-3})[u]	1.2 ± 0.3
GAUSSIAN	Energy (keV)[s]	3.98 ± 0.07
	σ (keV)[t]	$0.1^{+0.1}_{0}$
	Norm (10^{-4})[u]	$1.9^{+1.5}_{-1.1}$
	χ^2/dof	199.53/183

Notes. [a]Neutral column density; [b]multicolour accretion disc temperature; [c]normalization of the DISKBB; [d]blackbody temperature; [e]emission radius of the BLACKBODY; [f]photon index; [g]electrons temperature of the corona; [h]normalization of NTHCOMP; [i]photon index of the POWER-LAW; [j]normalization of the POWER-LAW; [k]energy of the absorption edge; [l]optical depth of the edge; [m]energy of the DISKLINE emission line; [n]power law dependence of emissivity; [o]inner radius in units of gravitational radii $R_{\rm g}$; [p]outer radius in units of gravitational radii $R_{\rm g}$; [q]inclination angle of the binary system; [r]normalization of the DISKLINE; [s]energy of the emission line; [t]broadening of the line; [u]normalization of the line.

Downloaded from https://academic.oup.com/mnras/article-abstract/457/3/2988/2588964 by Fabio Pintore on 09 May 2020

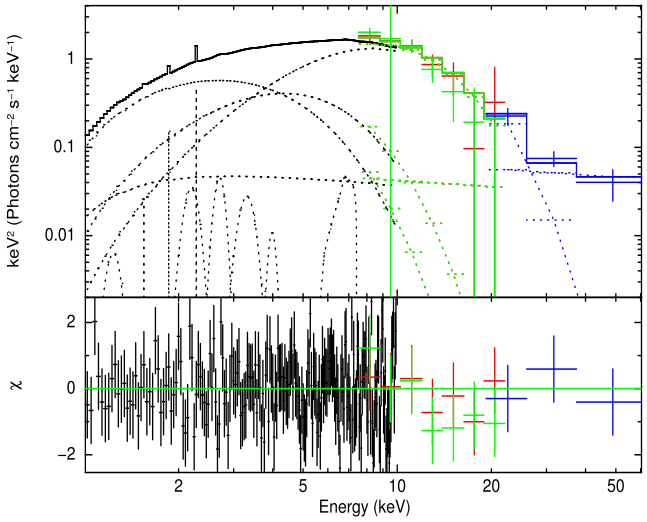

Figure 5. Unfolded $E^2f(E)$ *XMM–Newton*/EPIC-pn (black), *INTEGRAL*/JEMX-1 (red) and JEMX-2 (green) and *INTEGRAL*/ISGRI (blue). The dashed curves represent the best-fitting continuum (DISKBB, BB, NTHCOMP and POWER-LAW components) plus nine additional narrow and broad emission lines (see text).

parameters in Table 1 and show the best-fitting spectrum in Fig. 5.

If the large number of emission features is possibly associated with hard photons reflected from the disc, it suggests to fit the broad-band spectrum with a self-consistent reflection model. We test the REFLIONX (Ross & Fabian 2005) and the RFXCONV (e.g. Kolehmainen, Done & Díaz Trigo 2011) models. We remove the Fe DISKLINE model and we left only the GAUSSIAN models for those low-energy lines not included in the models (specifically Ar and Ca lines). Here we discuss only the RFXCONV model for sake of simplicity as the REFLIONX model gives very similar results. We convolve the RFXCONV with the RDBLUR model in order to take into account the relativistic effects. We find that the best-fitting model does not provide any statistical improvement (reduced χ^2 of 1.2) with respect to the fit with DISKLINE and GAUSSIAN models. Furthermore, the parameters of the RDBLUR are highly unconstrained. However the self-consistent model allows us to find that the reflection fraction is 0.094 ± 0.008, produced in a medium with an ionization of $\log \xi \sim 3.2$. We also tentatively let the iron abundance to vary but the fit resulted insensitive to any value assumed by the parameter. Hence, we cannot determine a stable continuum model for reflection and we should limit our discussion to the reflection fraction and the ionization parameter of the disc. Finally, we remark that, also with the self-consistent models, the hard POWER-LAW component is still requested by the spectral fit with an F-test probability of chance improvement $<10^{-5}$.

3.2 RGS

We avoid to fit the persistent RGS data (i.e. without bursts) together with the EPIC-pn spectrum using the same spectral model because of a clear discrepancy between RGS and EPIC-pn data. Although this is not dramatic, it introduces significant residuals in the simultaneous fit with the EPIC-pn data. We suspect this is not produced by a miscalibration of the EPIC-pn energy scale but rather from pile-up effects in the RGS and some other residuals miscalibration of these detectors. Indeed, following the standard procedure suggested in the *XMM–Newton* thread,[3] we infer that pile-up effects are present in these data.

We initially fit the stacked spectrum with an absorbed DISKBB model and we obtain a very poor fit (χ^2/dof = 2468.71/650; $nH \sim 0.57 \times 10^{22}$ cm^{-2} and $kT_{\rm disc} \sim 2$ keV). Large residuals are found in the fit, in particular around the neutral edges of Ne, Mg and Al. We may explain them as a mismatch in the depths associated with their neutral edges, probably due to the data being sensible to differences in the abundances of the different elements with respect to the adopted solar abundance table (Anders & Grevesse 1989). Therefore, we substitute the TBABS model, with the TBVARABS model, where it is possible to independently vary the abundance value for each element. We leave free to vary the abundance of Ne, Mg and Al and we found an improvement in the fit (χ^2/dof = 1557.14/647); the abundances of Ne and Mg converged towards ∼1.8 and ∼2.5 times the solar abundance, while the Al abundance was unlikely high (>10 times the solar abundance). The latter result suggests that the Al edge might not have an astrophysical nature and we very tentatively suggest instrumental effects, also related to the narrow Al emission line found in the EPIC-pn spectrum. In any case, residuals are still observed around the energies of these edges. To account for this issue, in TBVARABS we fix at zero the abundances of Ne, Mg and Al and we add three absorption edges to the model, leaving their energy and optical depth free to vary. This model further improves the fit (χ^2/dof = 1383.28/644), showing that the energies of Ne and Mg are slightly different but consistent within the uncertainties with those obtained in laboratory (Table 2). We note that the Ne edge can be also confused with the O VIII edge (0.871 keV), making the Ne more abundant of its actual value; the Al energy is instead very different (1.52 keV versus 1.564 keV). We finally add six narrow absorption lines which further lower the χ^2_ν (χ^2/dof = 1178.26/631; see Table 2 and Fig. 6). We identify at least the lines of Ne IX (0.922 keV), Na X (1.12 keV) and Mg XI (1.35 keV); a line found at 1.766 keV can be instead associated with a mismodelling of Mg IX edge (1.762 keV), while for the remaining two other lines (∼0.96 and 1.18 keV) the association was less certain. However, although we cannot find any other significant feature in the spectrum, the best fit is still poor and the residuals are still confused, especially around the Al edge (Fig. 6).

3.3 Burst analysis

The X-ray bursts in SAX J1748.9−2021 were associated with type-I bursts because of clear correlations of the blackbody temperature and the corresponding emitting radius during their rises and decays (Galloway et al. 2008; Güver & Özel 2013). The total number of X-ray bursts observed in the EPIC-pn data (TIMING mode) is 25, with a typical duration between the rise and the return to pre-burst rate of ∼100 s. We model the light curve of each burst with an exponential function and we find that the typical peak count rate is ∼1800 counts s^{-1} with an average decay folding time of $\tau = 61.1 \pm 0.7$ s. We note that the bursts occurred about one per hour; however, a more careful analysis shows that the elapsed time between a burst and the next presents an anticorrelation with the count rate right before the onset of the burst (Fig. 7, top). This suggests that, when the accretion rate increased, the rate of the bursts increased accordingly, as expected if the amount of matter needed to trigger the burst was more rapidly collected. In order to better investigate

[3] http://xmm.esac.esa.int/sas/current/documentation/threads/Pile-Up_in_the_RGS.shtml

Downloaded from https://academic.oup.com/mnras/article-abstract/457/3/2988/2588964 by Fabio Pintore on 09 May 2020

Table 2. RGS data, best-fitting spectral parameters obtained with the absorbed continuum DISKBB+NTHCOMP+POWER-LAW model, plus three absorption edge and six absorption lines. Errors are at 90 per cent for each parameter.

Model	Component	
TBABS	$N_{\rm H}$ (10^{22} cm^{-2})[a]	$0.572^{+0.002}_{-0.002}$
DISKBB	$kT_{\rm bb}$ (keV)[b]	$2.95^{+0.08}_{-0.3}$
	Norm.[c]	$5.59^{+0.01}_{-0.02}$
EDGE	Energy (keV)[d]	$0.8691^{+0.008}_{-0.007}$
	$\tau_{\rm edge}$[e]	$0.358^{+0.009}_{-0.008}$
EDGE	Energy (keV)[d]	$1.313^{+0.003}_{-0.002}$
	$\tau_{\rm edge}$[e]	$0.101^{+0.004}_{-0.007}$
EDGE	Energy (keV)[d]	$1.523^{+0.004}_{-0.006}$
	$\tau_{\rm edge}$[e]	$0.096^{+0.004}_{-0.005}$
GAUSSIAN	Energy (keV)[f]	0.923 ± 0.02
	Norm. (10^{-4})[g]	6 ± 2
GAUSSIAN	Energy (keV)[f]	0.963 ± 0.001
	Norm. (10^{-4})[g]	4.4 ± 2
GAUSSIAN	Energy (keV)[f]	$1.121^{+0.004}_{-0.002}$
	Norm. (10^{-4})[g]	4 ± 1
GAUSSIAN	Energy (keV)[f]	$1.177^{+0.008}_{-0.005}$
	Norm. (10^{-4})[g]	3 ± 1
GAUSSIAN	Energy (keV)[f]	$1.381^{+0.01}_{-0.009}$
	Norm. (10^{-4})[g]	2 ± 1
GAUSSIAN	Energy (keV)[f]	$1.7680^{+0.0009}_{-0.004}$
	Norm. (10^{-3})[g]	1.3 ± 0.2
	χ^2/dof	1178.26/631

Notes. [a]Neutral column density; [b]multicolour accretion disc temperature; [c]normalization of the DISKBB; [d]energy of the absorption edge; [e]optical depth of the edge; [f]energy of the emission line; [g]normalization of the line.

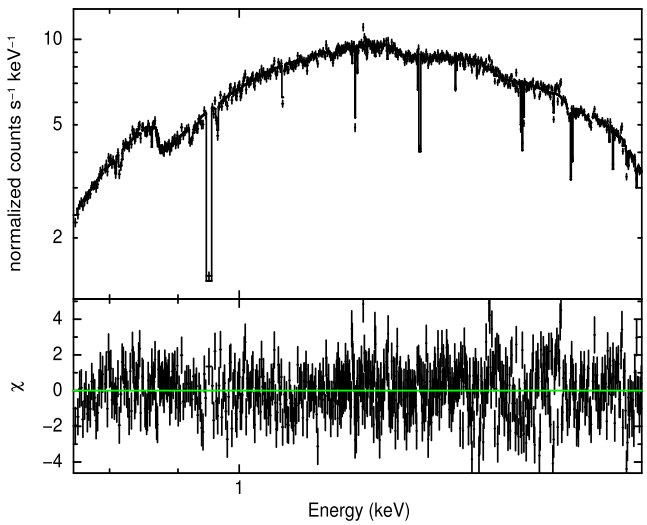

Figure 6. Unfolded $E^2f(E)$ *XMM–Newton*/RGS. A number of absorption features were added to the continuum and some edges were left free to vary (see text).

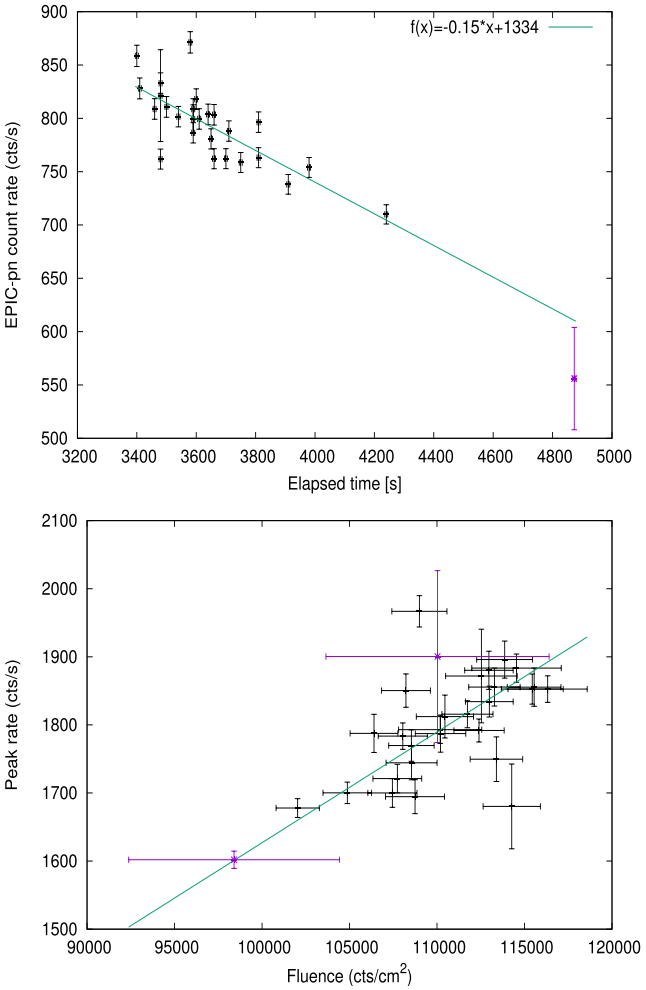

Figure 7. Top: pre-burst EPIC-pn count rate as a function of the elapsed time between a burst and the next one. A negative trend is observed. Bottom: peak count rate versus fluence in each burst observed during the *XMM–Newton* observation. In both plots, black points and purple crosses are bursts caught during the EPIC-pn TIMING mode and BURST mode, respectively. The green solid lines represent the best fit of the points.

this process, we also calculate the fluence of each burst (i.e. the total energy released during the burst) as a function of the type-I burst peak rate. In Fig. 7 (bottom), we show that the fluence increases with the burst peak rate, as expected if more material is deposited and burned on the NS surface. We note that the peak count rate does not show any saturation with the fluence, typical of bursts not reaching the Eddington limit (see e.g. Basinska et al. 1984): this may be an effect of the *XMM–Newton* counting mode because of telemetry saturation which was often triggered during the TIMING mode observation, leaving random gaps (of ∼8 s, on average) inside most of the bursts and hence possibly affecting the estimate of the total fluence. However, this effect is not present during the BURST mode light curve and we are able to estimate the correct total fluence, although with larger error bars because of the poorer statistics. In Fig. 7 (bottom), we show that the fluences calculated for both modes are consistent within the errors, suggesting the counting mode was not significantly contributing to the underestimation of the fluence. This result points towards the hypothesis that the type-I bursts did not reached the maximum peak luminosity (i.e. at the Eddington limit).

Downloaded from https://academic.oup.com/mnras/article-abstract/457/3/2988/2588964 by Fabio Pintore on 09 May 2020

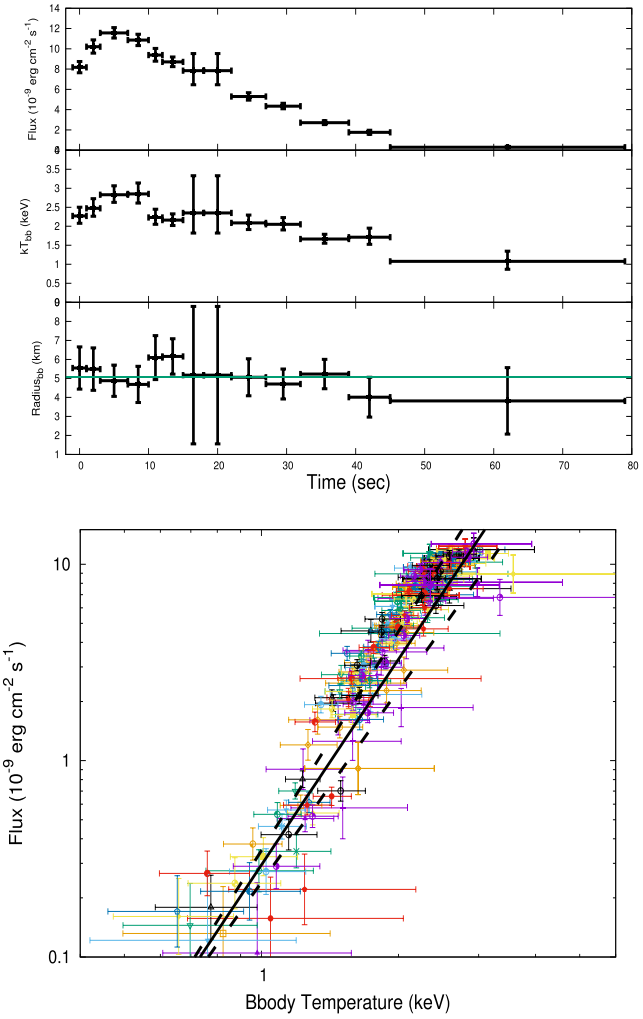

Figure 8. Top: evolution of the 0.3–10.0 keV flux (upper panel), the blackbody temperature (middle panel) and emission radius (lower panel) during a type-I burst. Bottom: evolution of the 0.3–10 keV flux as a function of the blackbody temperature during the bursts observed in the *XMM–Newton* observation. The black, solid line represents the best fit ($F_{0.3-10\,\mathrm{keV}} \propto T^{3.5\pm0.1}$), while the black, dashed lines its 3σ upper limits.

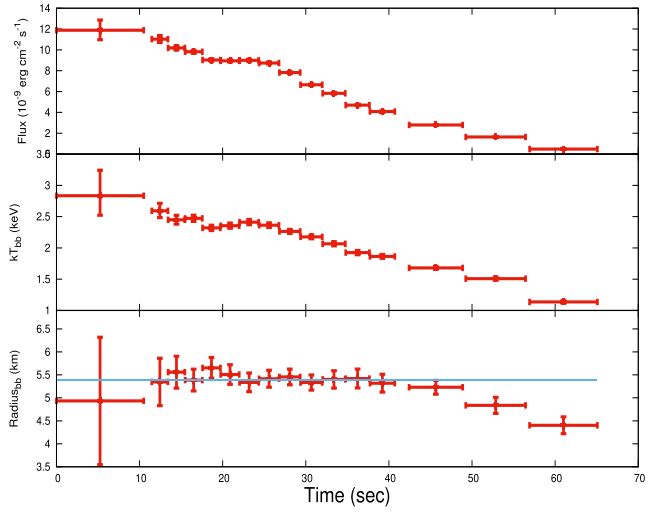

Figure 9. Evolution of the 0.3–10.0 keV flux (top panel), the blackbody temperature (centre panel) and emission radius (bottom panel) obtained by flux-bin spectra obtained by stacking all of the type-I bursts. Beyond 40/50 s after the peak the statistics of the single spectra is very low and the spectral parameters are not reliable. The emission radius, modified by the colour correction factor (1.35 ± 0.05), is consistent with a NS radius of 6.97–7.6 km.

In order to study the spectral evolution of the type-I bursts, for each of them we create a number of EPIC-pn spectra obtained by collecting photons from small intervals (from 2 to 15 s bin time according to the count rate) of their light curves. We use the averaged persistent spectrum as a background of the burst spectra, although this approach may be source of uncertainties (see e.g. Güver, Psaltis & Özel 2012a; Güver, Özel & Psaltis 2012b). We note that no short-term spectral variability was observed during the *XMM–Newton* observation allowing us to use the averaged persistent spectrum of the whole observation. We then fit each spectrum in the 1.0–10 keV energy range with an absorbed BLACKBODY model. Because we do not expect significant variability of the local absorbing materials around the source, we fix the absorption neutral column density to the best-fitting value of the persistent spectrum (5.8×10^{21} cm^{-2}). In Fig. 8 (top), we show the flux evolution of one of the type-I bursts (upper panel) and the corresponding blackbody temperature (middle panel) and radius (lower panel) evolution during the rise and the decay. The absorbed peak flux is around two/three times higher than the persistent flux, and the blackbody temperature increases up to ∼3 keV and then it decreases down to ∼1 keV at the end of the decay, although we note the large error bars. The statistics of the time-binned spectra do not allow to find evidence of a clear radius expansion, and we obtain that the radius of the emitting region is almost constant at ∼5 km. In addition, we show also the cooling tails of all of the X-ray bursts in Fig. 8 (bottom), where the flux follows a relation $F \propto T_{\mathrm{bb}}^{3.5\pm0.1}$, which is close to the expected $F \propto T_{\mathrm{bb}}^{4}$. The discrepancy between the theoretical and observed relation can arise from a slight variation of the blackbody radius during the burst, although we do not have enough statistics to prove it. We also remark that in Galloway et al. (2008) and Güver et al. (2012b), the authors reported only a subsample of type-I bursts of SAX J1748.9−2021 showing radius expansion at a touchdown flux of $\sim 4 \times 10^{-8}$ erg cm^{-2} s^{-1} in the energy range 2.5–25 keV. Extending our flux estimates to the same energy range, we evaluate an unabsorbed flux of 2.2×10^{-8} erg cm^{-2} s^{-1}, about a factor of 2 lower than the peak flux found in the *RXTE* data, although the peak temperatures result compatible. Therefore, the absence of a clear saturation for the fluence and the (on average) peak flux of 2.2×10^{-8} erg cm^{-2} s^{-1} suggest again that none of the type-I bursts observed in the *XMM–Newton* observation has reached the Eddington limit.

Since the spectral properties of the bursts are widely consistent amongst each other, in order to improve the signal-to-noise ratio, we create average flux-binned spectra obtained by stacking burst epochs at the same count rate. In this way, it was possible to find a clearer decay of the blackbody temperature from ∼3 down to ∼1.2 keV (Fig. 9), which is (as expected) very close to the blackbody temperature in the persistent spectrum (see Section 3.1). In addition, where the quality statistics is rich enough, the radius appears to be rather constant and consistent with 5.39 ± 0.03 km as no radius expansions are observed. Assuming a correction factor for the NS photosphere of 1.35 ± 0.05 (e.g. Madej, Joss & Różańska 2004; Majczyna et al. 2005; Güver et al. 2010a,b), the emitting radius allows us to constrain the NS radius at 6.97–7.6 km (assuming a distance of 8.5 kpc), consistent with the values reported in Güver & Özel (2013).

Downloaded from https://academic.oup.com/mnras/article-abstract/457/3/2988/2588964 by Fabio Pintore on 09 May 2020

4 DISCUSSION AND CONCLUSIONS

In this work, we have analysed in detail the spectral properties of the intermittent accreting millisecond pulsar SAX J1748.9−2021, during the brightest phase of its 2015 outburst. We made use of a high quality *XMM–Newton* observation, taken along the fast rise in flux of the outburst, and the stacking of 8 d *INTEGRAL* observations, taken around the peak of the outburst. The source showed an intense type-I X-ray burst activity (∼1 burst h^{-1} in the *XMM–Newton* observation) and, because they affect the persistent emission, we carried out a separate spectral analysis for the persistent and burst emission. The spectra of AMXPs are generally stable during the outbursts and can be well described by a multicomponents model, where the continuum is based on a Comptonization process of soft photons in a hot, optically thin electron population (kT_e ∼ 30–50 keV), possibly located close to the NS, plus a soft (<1 keV) component (widely accepted to be associated with the multicolour accretion disc) and, occasionally, a third thermal continuum component is also seen and likely produced by the NS surface (e.g. Gilfanov et al. 1998; Falanga et al. 2005; Gierliński & Poutanen 2005; Patruno et al. 2009b; Papitto et al. 2010, 2013a). However, in't Zand et al. (1999) studied a broad-band (0.1–100 keV) *BeppoSAX* spectrum of SAX J1748.9−2021 during the 1998 outburst and these authors reported that a single thermal Comptonization component was able to well describe the spectral properties of the source. The characteristics of such a component were consistent with an electron population temperature of ∼15 keV and optical depth of ∼3–6, fed by soft photons of ∼0.6 keV. However, no additional soft components were detected. Differently from the spectral state of SAX J1748.9−2021 observed by in't Zand et al. (1999) (likely a hard state), we found that the *XMM–Newton*+*INTEGRAL* data presented here show that the source was likely in a soft state, with a continuum based on two soft components (a DISKBB and a BBODY), which represent the multicolour accretion disc and the NS surface, respectively, a thermal Comptonization and a hard power-law tail. The thermal Comptonization component shows that the electron temperature is quite soft (kT_e ∼ 2.1 keV) and optically thick and it is fed by seed photons whose temperature is consistent with that of the blackbody component of the NS (∼1.1 keV). We could roughly estimate the emission radius of the seed photons, assuming a spherical emission radius for the seed photons and that most of them are scattered in the optically thick corona. Following in't Zand et al. (1999), we note that the emission radius of the seed photons can be calculated as $R_{\rm seed} = 3 \times 10^4\, d \sqrt{\frac{f_{\rm bol}}{1+y}}/(kT_{\rm seed})^2$, where d is the source distance, $f_{\rm bol}$ is the bolometric flux of the observed Comptonizing spectrum, y is the Compton parameter and $kT_{\rm seed}$ is the seed photons temperature. For a Compton parameter y of ∼36 (estimated by calculating the optical depth from kT_e and $\Gamma_{\rm compt}$ as shown in Zdziarski et al. 1996), an $f_{\rm bol}$ of $\sim 2.8 \times 10^{-9}$ erg cm^{-2} s^{-1}, a distance of 8.5 kpc and a seed photons temperature of ∼1.1 keV, we estimated that the emission radius is ∼2 ± 1 km, confirming a very small emitting region which may be possibly associated with a zone over the NS surface as the shock right above the accretion column. The temperature of the seed photons, similar to the NS temperature, and the size of the electron population strongly indicate that the Comptonizing medium is possibly located very close to the compact object. This may be further confirmed by the existence of a persistent pulsations in the *XMM–Newton* data (Sanna et al., submitted), which point towards the existence of a hotspot above the NS surface.

We calculated that the broad-band 1.0–50 keV absorbed (unabsorbed) flux is $\sim 4.9 \times 10^{-9}$ ($\sim 5.5 \times 10^{-9}$) erg cm^{-2} s^{-1}, consistent with a luminosity of $L_X \sim 4.2 \times 10^{37}$ erg s^{-1} ($\sim 4.7 \times 10^{37}$) (for a distance of 8.5 kpc), hence about 25 per cent of the Eddington luminosity for accretion on to a 1.4 $M_\odot$ compact object. The DISKBB, BBODY, NTHCOMP and POWER-LAW components represent the ∼20, 25, 51 and 3 per cent of the total unabsorbed flux, respectively. Moreover, SAX J1748.9−2021 was quite faint at very high energies (>10 keV), indicating that the source was clearly in a soft state, differently from most of the AMXPs spectra. Indeed, with the exception of the three intermittent millisecond sources which have also been caught during soft states, AMXPs are usually observed in spectral states consistent with hard states. Furthermore, it is interesting to note that persistent pulsators among AMXPs are generally observed pulsating during hard states, while the intermittent AMPXs have been seen pulsating in both hard and soft states (see e.g. Patruno & Watts 2012, and reference therein, for a review).

In addition, some emission features are found in the broad-band spectrum of the source, in particular broad emission lines of Fe, S, Ar and Ca. The broadening of the lines may suggest that they are produced by reflection off of hard photons from the surface of the disc and smeared by the fast motion of matter in the accretion disc. Broad emission lines have been found in several AMXPs (Papitto et al. 2009, 2010, 2013a; Cackett et al. 2010; Wilkinson et al. 2011; Cackett & Miller 2013) and they usually showed asymmetric profiles, which nature was associated with relativistic effects on reflected photons. From these lines, it was possible to estimate the radius at which they are produced, suggesting the existence of truncated accretion discs. Truncated discs are expected if the magnetic field is strong enough to drive the matter towards the NS magnetic polar caps. In our case, the Fe line (∼6.8 keV) was the strongest feature in the spectrum and we tentatively fitted it with a DISKLINE model which can provide information about the disc region where the line was formed. We found that the estimated best-fitting inner radius of the disc is comprised between 20 and $40R_g$ (∼40–80 km, assuming a NS of 1.4 $M_\odot$) with a disc inclined of 44° with respect to our line of sight. Also the intermittent-AMXP HETE 1900.1−2455 was characterized by an iron emission line at ∼6.6 keV and possibly originating at $25 \pm 15 R_g$ (Papitto et al. 2013a), consistent with the location of the iron line region in SAX J1748.9−2021. This result is quite intriguing as SAX J1748.9−2021 exhibited pulsations (persistently, as found by Sanna et al., submitted in the *XMM–Newton* data) during the reported soft state while the accreting millisecond pulsar HETE J1900.1−2455 in a burst occurred during an unusually soft state of the source showed only burst oscillations (Watts et al. 2009). However, HETE J1900.1−2455 has been also observed pulsating during hard states (Papitto et al. 2013a) unlike SAX J1748.9−2021 which, we highlight, pulsated only during soft states (Patruno et al. 2009a). In particular, it has been proposed that intermittency of HETE J1900.1−2455 is due to a magnetic field generally buried under the NS surface (Cumming 2008) or, if the magnetosphere is considered, to a breakthrough of accreting matter into the magnetic field lines, possibly accompanied by position changes of a hotspot located close to the spin axis of the NS (Romanova, Kulkarni & Lovelace 2008; Lamb et al. 2009). Other hypotheses suggest limitation of the pulse amplitude related to gravitational light bending effects (Özel 2009) or scattering of the coherent pulsation in an optically thick, hot corona around the NS (Titarchuk, Cui & Wood 2002). The truncation of the disc found by Papitto et al. (2013a) can be then possibly explained as an optically thin accretion flow in the regions closer to the NS, as also proposed for LMXB systems with non-pulsating NSs. However, such interpretations do not appear to be consistent with the characteristics of SAX J1748.9−2021.

Downloaded from https://academic.oup.com/mnras/article-abstract/457/3/2988/2588964 by Fabio Pintore on 09 May 2020

Therefore the two sources appear to behave in a different way and such considerations make SAX J1748.9−2021 a very peculiar source.

In fact, our results allow us to find a coherent picture for the source. A 3σ upper limit to the inner radius of the accretion disc would be ∼20 km, not very different from the 40–80 km inferred by the iron line with the DISKLINE model. The discrepancy between the two values may be due to very ionized inner regions of the disc, where the iron line cannot form. This inner disc radius implies that the matter does not reach the latest stable orbit, where the magnetic field would not be able to drive the accretion towards the polar cap (i.e. giving a truncated disc) and produce the persistent pulsating emission. Furthermore, the existence of a possible NS emission allows us to consider that the cold and optically thick corona does not hide the compact object. This would be expected in order to explain the pulsating emission, produced more likely in the polar caps.

We also remark the detection of a hard power-law tail, which carries ∼3 per cent of the total flux. Hard tails are very often observed in soft states of LMXB spectra (e.g. Di Salvo et al. 2000, 2001, 2006; D'Amico et al. 2001; Iaria et al. 2004; Paizis et al. 2006; D'Aí et al. 2007; Piraino et al. 2007; Tarana et al. 2007). During this state, the hard tails do not present high energy cut-off and they provide a small percentage of the total flux emission (a few per cent), although in the case of the accreting NS GX 3+1 such a component was found to carry up to ∼20 per cent of the total emission (Pintore et al. 2015). Several scenarios were proposed in order to explain hard tails: in particular, they can be either by non-thermal Comptonization of non-thermal, relativistic, electrons in a local outflow (e.g. Di Salvo et al. 2000) or in a corona (Poutanen & Coppi 1998), or by the bulk motion of accreting material close to the NS (e.g. Titarchuk & Zannias 1998). Another scenario suggests synchrotron emission from a relativistic jet escaping from the system (Markoff, Falcke & Fender 2001) and, in the second scenario, theory expects also that radio emission would be observed (e.g. Homan et al. 2004; Migliari et al. 2007), although for SAX J1748.9−2021 such a detection is still not confirmed. Future simultaneous multiwavelength observations of the source, in particular X-ray and radio, will be very useful to further investigate the nature of such a component.

Despite of the reported results and although emission lines and continuum properties are consistent, we found difficulties to find robust spectral fits when describing the broad-band spectrum with a reflection continuum adopting self-consistent models (as REFLIONX or RFXCONV). Hence, our results cannot strongly rule out the possibility that the emission lines are instead broadened by Compton down-scattering due to a narrow wind shell ejected at mildly relativistic velocities at some disc radii where the local radiation force overcomes the local disc gravity (Laurent & Titarchuk 2007) or, as another possible scenario, by Compton processes in a moderately, optically thick accretion disc corona (ADC) generated for evaporation above the accretion disc (White & Holt 1982; Kallman & White 1989; Vrtilek, Soker & Raymond 1993). However, in the latter case, the broadening of the line and the temperature of the electron population should be related with $\Delta\epsilon/\epsilon = (4kT_{\rm e} - \epsilon)/m_{\rm e}c^2$. From this relation, the electron temperature should be ∼9.5 keV, more than a factor of 4 higher than the temperature obtained with the NTHCOMP model. Hence, we would favour an interpretation of the SAX J1748.9−2021 emission lines in terms of reflection. Assuming that the fits obtained adopting self-consistent models (although not completely stable) are reliable, we can make some considerations about the nature of the process. In particular, we could find that the ionization level ξ of the reflector is consistent with ∼1600 erg cm s^{-1}; hence, from the relation $\xi = L/nR^2$ (where L is the unabsorbed X-ray luminosity of the illuminating source, n is the number density of the reflecting medium and R is the distance from the reflector), we estimate a distance from the reflector of ∼50 km, assuming a hydrogen density of 5×10^{20} cm^{-3} (as expected from the Shakura–Sunyaev model for accretion around a NS; Ross & Fabian 2007). The distance is well consistent with that inferred from the DISKLINE model and, because at ∼50 km from the NS surface the relativistic effects are less pronounced, this can explain why we could not robustly constrain most of the parameters of the relativistic kernel (RDBLUR).

Finally, we investigated the numerous type-I X-ray bursts present in the *XMM–Newton* observation. We found a clear evolution of the blackbody temperature during bursts, with a peak temperature around 3 keV, although we could not find any 'touchdown' moment because of the limited statistics. The relation between fluence and peak count rate suggests that none of the type-I X-ray bursts was able to reach the Eddington limit. However, it was possible to estimate the radius which is responsible for the emission of such a blackbody component, inferring a value of 7.0–7.6 km (assuming a distance of 8.5 kpc). This value is consistent within the error of the previous estimates (8.18 ± 1.6 or 10.93 ± 2.09 km; Güver & Özel 2013) obtained by analysing *RXTE* data. The average unabsorbed 0.3–10 keV peak flux is $\sim 1.2 \times 10^{-8}$ erg cm^{-2} s^{-1}, corresponding to a 0.3–10 keV luminosity of 1×10^{38} erg s^{-1} (assuming a distance of 8.5 kpc). This value indicates that the burst reached a peak luminosity of ∼50 per cent of the Eddington luminosity for a 1.4 $M_\odot$ NS.

ACKNOWLEDGEMENTS

We thank N. Schartel, who made this ToO observation possible in the Director Discretionary Time, and the *XMM–Newton* team who performed and supported this observation. We also thank the unknown referee for help in improving the paper. Authors acknowledge financial contribution from the agreement ASI-INAF I/037/12/0. We gratefully acknowledge the Sardinia Regional Government for the financial support (P. O. R. Sardegna F.S.E. Operational Programme of the Autonomous Region of Sardinia, European Social Fund 2007–2013 – Axis IV Human Resources, Objective l.3, Line of Activity l.3.1). This work was partially supported by the Regione Autonoma della Sardegna through POR-FSE Sardegna 2007–2013, L.R. 7/2007, Progetti di Ricerca di Base e Orientata, Project N. CRP-60529. The High-Energy Astrophysics Group of Palermo acknowledges support from the Fondo Finalizzato alla Ricerca (FFR) 2012/13, project N. 2012-ATE-0390, founded by the University of Palermo. MDS thanks the Dipartimento di Fisica e Chimica, Universita' di Palermo, for the hospitality.

REFERENCES

Altamirano D., Casella P., Patruno A., Wijnands R., van der Klis M., 2008, ApJ, 674, L45
Anders E., Grevesse N., 1989, Geochim. Cosmochim. Acta, 53, 197
Archibald R. F., Kaspi V. M., Beardmore A. P., Gehrels N., Kennea J. A., 2015, ApJ, 810, 67
Arnaud K. A., 1996, in Jacoby G. H., Barnes J., eds, ASP Conf. Ser. Vol. 101, Astronomical Data Analysis Software and Systems V. Astron. Soc. Pac., San Francisco, p. 17
Balucinska-Church M., McCammon D., 1992, ApJ, 400, 699
Basinska E. M., Lewin W. H. G., Sztajno M., Cominsky L. R., Marshall F. J., 1984, ApJ, 281, 337
Bhattacharya D., van den Heuvel E. P. J., 1991, Phys. Rep., 203, 1

Downloaded from https://academic.oup.com/mnras/article-abstract/457/3/2988/2588964 by Fabio Pintore on 09 May 2020

Bouchet L., del Santo M., Jourdain E., Roques J. P., Bazzano A., DeCesare G., 2009, ApJ, 693, 1871
Bozzo E., Kuulkers E., Ferrigno C., 2015a, Astron. Telegram, 7106
Bozzo E., Falanga M., Ferrigno C., 2015b, Astron. Telegram, 7136
Burderi L., Di Salvo T., 2013, Mem. Soc. Astron. Ital., 84, 117
Burderi L., King A. R., 1998, ApJ, 505, L135
Cackett E. M., Miller J. M., 2013, ApJ, 777, 47
Cackett E. M. et al., 2010, ApJ, 720, 205
Casella P., Altamirano D., Patruno A., Wijnands R., van der Klis M., 2008, ApJ, 674, L41
Courvoisier T. J.-L. et al., 2003, A&A, 411, L53
Cumming A., 2008, in Wijnands R., Altamirano D., Soleri P., Degenaar N., Rea N., Casella P., Patruno A., Linares M., eds, AIP Conf. Ser. Vol. 1068, A Decade of Accreting Millisecond X-ray Pulsars. Am. Inst. Phys., New York, p. 152
D'Aí A., Życki P., Di Salvo T., Iaria R., Lavagetto G., Robba N. R., 2007, ApJ, 667, 411
D'Amico F., Heindl W. A., Rothschild R. E., Gruber D. E., 2001, ApJ, 547, L147
Del Santo M., 2012, J. Phys. Conf. Ser., 354, 012003
Del Santo M., Malzac J., Jourdain E., Belloni T., Ubertini P., 2008, MNRAS, 390, 227
Del Santo M. et al., 2015, preprint (arXiv:e-prints)
Dickey J. M., Lockman F. J., 1990, ARA&A, 28, 215
Di Salvo T. et al., 2000, ApJ, 544, L119
Di Salvo T., Robba N. R., Iaria R., Stella L., Burderi L., Israel G. L., 2001, ApJ, 554, 49
Di Salvo T. et al., 2006, ApJ, 649, L91
di Salvo T. et al., 2009, MNRAS, 398, 2022
Fabian A. C., Rees M. J., Stella L., White N. E., 1989, MNRAS, 238, 729
Falanga M. et al., 2005, A&A, 444, 15
Galloway D. K., Morgan E. H., Krauss M. I., Kaaret P., Chakrabarty D., 2007, ApJ, 654, L73
Galloway D. K., Muno M. P., Hartman J. M., Psaltis D., Chakrabarty D., 2008, ApJS, 179, 360
Gavriil F. P., Strohmayer T. E., Swank J. H., Markwardt C. B., 2007, ApJ, 669, L29
Ghosh P., Becker W., 2008, Phys. Today, 61, 60
Gierliński M., Poutanen J., 2005, MNRAS, 359, 1261
Gilfanov M., Revnivtsev M., Sunyaev R., Churazov E., 1998, A&A, 338, L83
Güver T., Özel F., 2013, ApJ, 765, L1
Güver T., Özel F., Cabrera-Lavers A., Wroblewski P., 2010a, ApJ, 712, 964
Güver T., Wroblewski P., Camarota L., Özel F., 2010b, ApJ, 719, 1807
Güver T., Psaltis D., Özel F., 2012a, ApJ, 747, 76
Güver T., Özel F., Psaltis D., 2012b, ApJ, 747, 77
Homan J., Wijnands R., Rupen M. P., Fender R., Hjellming R. M., di Salvo T., van der Klis M., 2004, A&A, 418, 255
Iaria R., Di Salvo T., Robba N. R., Burderi L., Stella L., Frontera F., van der Klis M., 2004, ApJ, 600, 358
in't Zand J. J. M. et al., 1999, A&A, 345, 100
in't Zand J. J. M., van Kerkwijk M. H., Pooley D., Verbunt F., Wijnands R., Lewin W. H. G., 2001, ApJ, 563, L41
Kaaret P., Morgan E. H., Vanderspek R., Tomsick J. A., 2006, ApJ, 638, 963
Kallman T., White N. E., 1989, ApJ, 341, 955
Kolehmainen M., Done C., Díaz Trigo M., 2011, MNRAS, 416, 311
Kuulkers E., den Hartog P. R., in't Zand J. J. M., Verbunt F. W. M., Harris W. E., Cocchi M., 2003, A&A, 399, 663
Kuulkers E. et al., 2015, Astron. Telegram, 7098
Lamb F. K., Boutloukos S., Van Wassenhove S., Chamberlain R. T., Lo K. H., Miller M. C., 2009, ApJ, 705, L36
Laurent P., Titarchuk L., 2007, ApJ, 656, 1056
Lebrun F. et al., 2003, A&A, 411, L141
Lund N. et al., 2003, A&A, 411, L231
McClintock J. E., Remillard R. A., 2006, in Levin W. H. G., van der Klis M., eds, Compact Stellar X-ray Sources. Cambridge Univ. Press, Cambridge, p. 157
Madej J., Joss P. C., Różańska A., 2004, ApJ, 602, 904
Majczyna A., Madej J., Joss P. C., Różańska A., 2005, A&A, 430, 643
Markert T. H., Backman D. E., Canizares C. R., Clark G. W., Levine A. M., 1975, Nature, 257, 32
Markoff S., Falcke H., Fender R., 2001, A&A, 372, L25
Markwardt C. B., Swank J. H., 2005, Astron. Telegram, 495, 1
Martins D. H., Harvel C. A., Miller D. H., 1980, AJ, 85, 521
Messenger C., Patruno A., 2015, ApJ, 806, 261
Migliari S. et al., 2007, ApJ, 671, 706
Mitsuda K. et al., 1984, PASJ, 36, 741
Ortolani S., Barbuy B., Bica E., 1994, A&AS, 108, 653
Özel F., 2009, ApJ, 691, 1678
Paizis A. et al., 2006, A&A, 459, 187
Papitto A., Di Salvo T., D'Aì A., Iaria R., Burderi L., Riggio A., Menna M. T., Robba N. R., 2009, A&A, 493, L39
Papitto A., Riggio A., di Salvo T., Burderi L., D'Aì A., Iaria R., Bozzo E., Menna M. T., 2010, MNRAS, 407, 2575
Papitto A. et al., 2013a, MNRAS, 429, 3411
Papitto A. et al., 2013b, Nature, 501, 517
Patruno A., Watts A. L., 2012, preprint (arXiv:e-prints)
Patruno A., Altamirano D., Hessels J. W. T., Casella P., Wijnands R., van der Klis M., 2009a, ApJ, 690, 1856
Patruno A., Rea N., Altamirano D., Linares M., Wijnands R., van der Klis M., 2009b, MNRAS, 396, L51
Pintore F. et al., 2014, MNRAS, 445, 3745
Pintore F. et al., 2015, MNRAS, 450, 2016
Piraino S., Santangelo A., di Salvo T., Kaaret P., Horns D., Iaria R., Burderi L., 2007, A&A, 471, L17
Poutanen J., 2006, Adv. Space Res., 38, 2697
Poutanen J., Coppi P. S., 1998, Phys. Scr., T77, 57
Poutanen J., Svensson R., 1996, ApJ, 470, 249
Romanova M. M., Kulkarni A. K., Lovelace R. V. E., 2008, ApJ, 673, L171
Ross R. R., Fabian A. C., 2005, MNRAS, 358, 211
Ross R. R., Fabian A. C., 2007, MNRAS, 381, 1697
Tarana A., Bazzano A., Ubertini P., Zdziarski A. A., 2007, ApJ, 654, 494
Titarchuk L., Zannias T., 1998, ApJ, 493, 863
Titarchuk L., Cui W., Wood K., 2002, ApJ, 576, L49
Valenti E., Ferraro F. R., Origlia L., 2007, AJ, 133, 1287
Verbunt F., van Kerkwijk M. H., in't Zand J. J. M., Heise J., 2000, A&A, 359, 960
Vrtilek S. D., Soker N., Raymond J. C., 1993, ApJ, 404, 696
Watts A. L. et al., 2009, ApJ, 698, L174
White N. E., Holt S. S., 1982, ApJ, 257, 318
Wijnands R., van der Klis M., 1998, Nature, 394, 344
Wilkinson T., Patruno A., Watts A., Uttley P., 2011, MNRAS, 410, 1513
Zdziarski A. A., Johnson W. N., Magdziarz P., 1996, MNRAS, 283, 193
Życki P. T., Done C., Smith D. A., 1999, MNRAS, 309, 561

This paper has been typeset from a TEX/LATEX file prepared by the author.

Downloaded from https://academic.oup.com/mnras/article-abstract/457/3/2988/2588964 by Fabio Pintore on 09 May 2020